Acta Crystallographica Section F
Structural Biology and Crystallization Communications
ISSN 1744-3091

Cloning, expression, purification, crystallization and preliminary X-ray crystallographic analysis of the TIR domain from the *Brucella melitensis* TIR-domain-containing protein TcpB

Mohammed Alaidarous,[a,b,c] Thomas Ve,[a,b,c] M. Obayed Ullah,[a,b,c] Eugene Valkov,[d] Ashley Mansell,[e] Mark A. Schembri,[a,c] Matthew J. Sweet[b,c] and Bostjan Kobe[a,b,c]*

[a]School of Chemistry and Molecular Biosciences, University of Queensland, Brisbane, QLD 4072, Australia, [b]Institute for Molecular Bioscience, University of Queensland, Brisbane, QLD 4072, Australia, [c]Australian Infectious Diseases Research Centre, University of Queensland, Brisbane, QLD 4072, Australia, [d]MRC Laboratory of Molecular Biology, Cambridge, CB2 0QH, England, and [e]Centre for Innate Immunity and Infectious Diseases, Monash Institute of Medical Research, Monash University, Melbourne, VIC 3168, Australia

Correspondence e-mail: b.kobe@uq.edu.au

Received 8 August 2013
Accepted 2 September 2013

In mammals, Toll-like receptors (TLRs) recognize conserved microbial molecular signatures and induce an early innate immune response in the host. TLR signalling is mediated by interactions between the cytosolic TIR (*T*oll/*i*nterleukin-1 *r*eceptor) domains of the receptor and the adaptor proteins. Increasingly, it is apparent that pathogens target this interaction *via* pathogen-expressed TIR-domain-containing proteins to modulate immune responses. A TIR-domain-containing protein TcpB has been reported in the pathogenic bacterium *Brucella melitensis*. Studies have shown that TcpB interferes with the TLR2 and TLR4 signalling pathways to inhibit TLR-mediated inflammatory responses. Such interference may involve TIR–TIR-domain interactions between bacterial and mammalian proteins, but there is a lack of information about these interactions at the molecular level. In this study, the cloning, expression, purification, crystallization and preliminary X-ray crystallographic analysis of the protein construct corresponding to the TIR domain of TcpB (residues 120–250) are reported. The crystals diffracted to 2.6 Å resolution, have the symmetry of the monoclinic space group $P2_1$ and are most likely to contain four molecules in the asymmetric unit. The structure should help in understanding the molecular basis of how TcpB affects the innate immunity of the host.

1. Introduction

Toll-like receptors (TLRs) recognize conserved microbial molecules and initiate innate immune responses in mammalian hosts (Gay & Gangloff, 2007). The C-terminal TIR domain is found in all mammalian TLRs and several cytosolic adaptor proteins (Ve *et al.*, 2012). TIR-domain homodimerization or heterodimerization is important for the activation of downstream signalling and the induction of transcription factors such as nuclear factor-κB (NF-κB) and interferon regulatory factors (IRFs) (Ve *et al.*, 2012). Activation of these transcription factors initiates pro-inflammatory cytokine secretion, which recruits more immune cells to the site of infection (Kawai & Akira, 2007) with the aim of clearing the pathogen threat. A number of human TIR-domain protein structures have been determined. The structures of the TIR domains from TLR1, TLR2, TLR10, IL-1RAPL receptors and the adaptor proteins MAL/TIRAP and MyD88 have been determined (Xu *et al.*, 2000; Nyman *et al.*, 2008; Valkov *et al.*, 2011; Khan *et al.*, 2004; Ohnishi *et al.*, 2009; Snyder *et al.*, 2013; Lin *et al.*, 2012). TIR-domain-containing protein structures have also been reported from the bacterium *Paracoccus denitrificans* (PdTIR; Chan *et al.*, 2009) and plants: *Arabidopsis thaliana* (AtTIR) and the flax-resistance protein L6 (Chan *et al.*, 2010; Bernoux *et al.*, 2011). All TIR domains are characterized by a globular fold containing a central core of parallel β-sheets surrounded by α-helices and connected by loop regions (Ve *et al.*, 2012).

Owing to the critical nature of TIR–TIR-domain interactions in TLR-mediated signalling and inflammatory responses, this interaction has been the source of 'targeting' by pathogens as a means of modulating the innate immune response and facilitating immune escape (Xiao, 2010; Bowie & Unterholzner, 2008). A number of pathogenic bacteria use TIR-domain-containing proteins to actively interfere with TLR signalling (Rana *et al.*, 2012). Different mechanisms have been proposed for the role of TIR-domain-containing protein homologues in the interference with the host innate immune

response (Rana *et al.*, 2012). Newman and coworkers were first to report the inhibitory effect of *Salmonella enterica* serovar Enteritidis TIR-domain-containing protein A (TlpA) on NF-κB activation, which was reported to interfere with the TLR4 and MyD88 signalling pathways (Newman *et al.*, 2006). Later studies identified two TIR-domain-containing proteins in uropathogenic *Escherichia coli* (TcpC) and *Brucella melitensis* (TcpB) (Cirl *et al.*, 2008). Both TcpC and TcpB were found to interfere with TLR2-mediated and TLR4-mediated NF-κB activation and the secretion of pro-inflammatory cytokines (Yadav *et al.*, 2010; Radhakrishnan & Splitter, 2010). Co-immunoprecipitation studies showed interaction between purified TcpC-TIR and ectopically expressed MyD88, suggesting that direct protein–protein interactions are implicated in the suppression of the innate immune response (Cirl *et al.*, 2008).

TcpB was recently reported to be involved in inhibiting the maturation of infected dendritic cells, which consequently reduces the production of pro-inflammatory cytokines (Salcedo *et al.*, 2008). The protein was suggested to mimic MAL/TIRAP by binding to the plasma membrane *via* its N-terminal PIP2 (phosphatidylinositol 4,5-bisphosphate) binding domain and competitively interacting with MyD88 (Radhakrishnan *et al.*, 2009). This may support the finding by Cirl and coworkers, who reported that TcpB interacts with endogenous MyD88 in HEK293 cells (Cirl *et al.*, 2008). However, in later studies Sengupta and coworkers proposed that TcpB interacts only with MAL/TIRAP and does not interfere with MAL/TIRAP–MyD88 interactions (Sengupta *et al.*, 2010). It was also shown that TcpB reduces MAL/TIRAP expression in HEK293 cells and enhances the ubiquitination and degradation of MAL/TIRAP (Sengupta *et al.*, 2010). Overall, there is no agreement in the literature as to whether TcpB interacts with the adaptor proteins (MyD88 or Mal/TIRAP) or with the TLRs (TLR4 or TLR2) (Cirl *et al.*, 2008; Radhakrishnan *et al.*, 2009; Sengupta *et al.*, 2010; Chaudhary *et al.*, 2012), and this is compounded by the indirect nature of some of the assays used.

To shed light on the molecular basis of TcpB function, we initiated a structural analysis of this protein. Here we report the molecular cloning, expression, purification, crystallization and preliminary X-ray crystallographic analysis of the TIR domain from *Brucella melitensis* TcpB.

2. Experimental methods

2.1. Cloning

The DNA sequences encoding residues 70–250 and 120–250 of TcpB (hereafter referred to as TcpBΔ70 and TcpBΔ120, respectively) were amplified by PCR and ligated into the pMCSG7 vector using ligation-independent cloning (Eschenfeldt *et al.*, 2009). The resulting constructs included an N-terminal His_6 tag followed by a TEV protease cleavage site. The correct DNA sequences were verified by sequencing.

2.2. Protein expression and purification

TcpBΔ70 and TcpBΔ120 were expressed using the auto-induction method (Studier, 2005). Transformed *Escherichia coli* BL21 (DE3) cells were propagated at 310 K until the mid-logarithmic phase ($OD_{600\ nm}$ of approximately 0.8) was reached. The temperature was then reduced to 288 K and the cells were grown overnight. The next day, the cells were harvested by centrifugation at 7500*g* (JLA-9.1000 rotor, Beckman Coulter) for 10 min, resuspended in 5 ml lysis buffer per gram of cell pellet (lysis buffer: 50 m*M* Tris base pH 8.0, 500 m*M* NaCl, 20 m*M* imidazole). The cells were lysed using sonication (40% amplitude, 10 s pulse on/10 s pulse off for 1 min at 277 K) and cell debris was removed by centrifugation at 27 200*g* (JA-20 rotor, Beckman Coulter) for 40 min. The resulting supernatant was applied onto a HisTrap FF 5 ml column (GE Healthcare) pre-equilibrated with lysis buffer. The bound protein was eluted using a 20–300 m*M* imidazole gradient. Fractions containing the protein of interest were pooled, buffer-exchanged into TEV cleavage buffer (50 m*M* Tris–HCl pH 8.0, 250 m*M* NaCl, 1 m*M* DTT, 0.5 m*M* EDTA) and treated with TEV protease overnight at 277 K. The cleaved protein was then applied onto the HisTrap FF 5 ml column for a second time to remove the cleaved His_6 tag, the TEV protease and other contaminants. The flowthrough was concentrated and loaded onto a Superdex 75 HiLoad 26/60 gel-filtration column (GE Healthcare) pre-equilibrated with 50 m*M* HEPES pH 8.0, 250 m*M* NaCl, 1 m*M* DTT. Peak fractions were pooled, concentrated (using Amicon Ultra-15 10K, Millipore) to final concentrations of 8–10 mg ml^{-1} for TcpBΔ70 and 10–22 mg ml^{-1} for TcpBΔ120, and stored in aliquots at 193 K. The purity of the protein was assessed using SDS–PAGE.

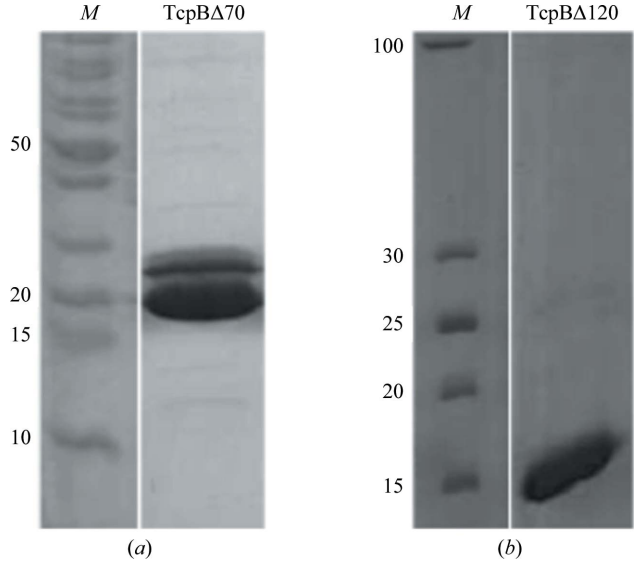

Figure 1
SDS–PAGE analysis of purified TcpBΔ70 (*a*) and TcpBΔ120 (*b*) following a two-step chromatography purification. Lane *M* contains molecular-mass markers (labelled in kDa).

2.3. Crystallization, data collection and processing

Several commercially available crystallization screens including Index, PEG/Ion and PEGRx (Hampton Research), Morpheus, JCSG+, ProPlex and PACT Premier (Molecular Dimensions), Systematically Controlled Crystallization Screen Set 101 (Axygen Biosciences) and Precipitant Synergy Crystallization Screen (Emerald BioSystems) were used to identify possible crystallization conditions. The hanging-drop vapour-diffusion method was used at 293 K and drops were set up using a Mosquito robot (TTP LabTech, UK) at the UQ-ROCX Diffraction Facility. Each drop consisted of 100 nl protein solution and 100 nl reservoir solution and was equilibrated against 75 µl reservoir solution. Plates were stored in an automated imaging system (Rock Imager, Formulatrix, USA) and images were taken after 0, 0.5, 1, 2, 3, 5, 8, 13 and 21 d. Hits from the initial crystallization screens were optimized by varying the protein concentration, the precipitant concentration and the pH.

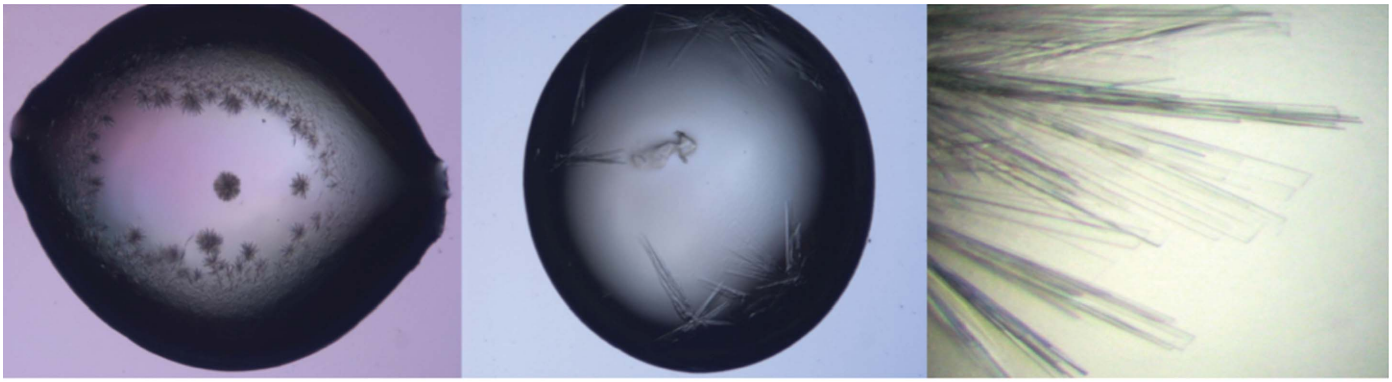

(*a*) (*b*) (*c*)

Figure 2
TcpBΔ70 crystal optimization. (*a*) Initial crystals in Morpheus (condition D5). (*b*) The best drop containing crystals after pH and precipitant concentration optimization [obtained using a condition consisting of 0.1 *M* HEPES pH 7.5, 30%(*w*/*v*) PEG 3350]. (*c*) Crystals after additive screening and pH optimization [obtained using a condition consisting of 0.1 *M* HEPES pH 5.5, 30%(*w*/*v*) PEG 3350, 10%(*v*/*v*) 2-propanol].

Several cryoprotectants were selected from Kempkes *et al.* (2008). PEG 3350, PEG 400, glycerol and MPD were tested for successful vitrification. Glycerol was the best and it was used for crystal cryopreservation. Single crystals of TcpBΔ70 and TcpBΔ120 were mounted in nylon loops and soaked in mother-liquor solution containing ∼25% glycerol prior to flash-cooling in liquid nitrogen. X-ray data were only collected from a TcpBΔ120 crystal under cryogenic conditions (100 K) on the Australian Synchrotron MX2 beamline using a wavelength of 0.953693 Å. The crystal-to-detector distance was set to 399 mm and 360 images were collected with an oscillation range of 1.0°. The data were collected using the *Blu-Ice* software (McPhillips *et al.*, 2002); *XDS* (Kabsch, 2010) and *SCALA* (within the *CCP*4 suite; Winn *et al.*, 2011) were used for data indexing/integration and scaling, respectively.

3. Results and discussion

Several TcpB TIR-domain constructs were screened for expression and solubility. Constructs encompassing amino-acid residues 70–250 (TcpBΔ70) and 120–250 (TcpBΔ120) were successfully expressed as soluble proteins in *E. coli* and were purified to homogeneity using a combination of immobilized metal-ion affinity chromatography and gel filtration. The purity of both proteins was approximately 95% as observed by SDS–PAGE (Fig. 1). Initial crystallization screening was carried out using a protein concentration of ∼10 mg ml^{-1} for both TcpBΔ70 and TcpBΔ120. Crystallization screening led to several promising conditions for TcpBΔ70 but not TcpBΔ120. Therefore, crystal optimization was carried out using TcpBΔ70.

The best initial hit for TcpBΔ70 corresponded to Morpheus condition D5. The crystals had a needle-like shape and grew in clusters. Optimization was carried out by using solutions with different pH values (in the range pH 4–9) and different PEGs (PEG 20 000, PEG 8000, PEG 6000 and PEG 3350) at a range of concentrations (5–35%). Crystals grew without adding volatiles in a condition consisting of 0.1 *M* HEPES pH 7.5, 30%(*w*/*v*) PEG 3350. In comparison to other PEGs, PEG 3350 reduced mass nucleation. Further optimization using micro-seeding was performed but without success. Therefore, we screened volatile additives in the Hampton Research Additive Screen. The crystal morphology was slightly improved by using 2-propanol, but the clustering morphology could not be avoided. Further optimization was carried out using solutions with different pH values (in the range pH 4–9) and different concentrations of PEG 3350 (5–35%) and 2-propanol (1–20%). A single crystal (obtained by gently separating the crystal cluster), grown using a protein concentration of 8 mg ml^{-1} in a condition consisting of 0.1 *M* HEPES pH 5.5, 30%(*w*/*v*) PEG 3350, 10%(*v*/*v*) 2-propanol (Fig. 2), was used for data collection. Unfortunately, the crystal did not diffract beyond 8 Å resolution.

Figure 3
Plate-like crystals of TcpBΔ120 [obtained using a condition consisting of 0.1 *M* bis-tris pH 5.5, 0.2 *M* NaCl, 25%(*w*/*v*) PEG 3350].

Additional screens were therefore performed using TcpBΔ120. A large number of drops in the initial screen were clear, suggesting that the protein concentration was too low. Therefore, we increased the concentration of TcpBΔ120 to 22 mg ml^{-1} and repeated the initial screening using freshly purified protein. Plate-like crystals (Fig. 3) were observed in one condition consisting of 0.1 *M* bis-tris pH 5.5, 0.2 *M* NaCl, 25%(*w*/*v*) PEG 3350 (Index condition No. 70). Unfortunately, these crystals could not be reproduced. The reason could be that we used thawed protein aliquots instead of fresh protein for crystal optimization. Therefore, we used the crystals from this screening for X-ray data collection at the Australian Synchrotron.

A single TcpBΔ120 crystal (Fig. 3) diffracted to 2.6 Å resolution and analysis of the diffraction data using *POINTLESS* (Evans, 2006) identified a monoclinic lattice and $P2_1$ as the most likely space group based on the analysis of systematic absences. The unit-cell parameters

Table 1
Crystal and data-collection statistics for TcpBΔ120.

Values in parentheses are for the outermost resolution shell.

No. of crystals	1
Beamline	MX2, Australian Synchrotron
Wavelength (Å)	0.953693
Detector	ADSC Quantum 315r
Crystal-to-detector distance (mm)	339
Rotation range per image (°)	1.0
No. of images	360
Space group	$P2_1$
Unit-cell parameters (Å, °)	a = 51.97, b = 73.68, c = 74.76, β = 93.29
Molecules per asymmetric unit	4
Resolution limits (Å)	52.43–2.71 (2.57–2.71)
No. of unique observations	18090
Completeness (%)	100.0 (99.7)
Multiplicity	3.7 (3.7)
$R_{\rm merge}$† (%)	8.9 (79.0)
$R_{\rm p.i.m.}$‡ (%)	5.4 (48.3)
Average $I/\sigma(I)$	10.6 (1.9)

† $R_{\rm merge} = \sum_{hkl}\sum_i |I_i(hkl) - \langle I(hkl)\rangle| / \sum_{hkl}\sum_i I_i(hkl)$, where $I_i(hkl)$ is the intensity of an individual measurement of the reflection with Miller indices hkl and $\langle I(hkl)\rangle$ is the mean intensity of that reflection. ‡ $R_{\rm p.i.m.} = \sum_{hkl}\{1/[N(hkl)-1]\}^{1/2}\sum_i |I_i(hkl) - \langle I(hkl)\rangle| / \sum_{hkl}\sum_i I_i(hkl)$.

were a = 51.97, b = 73.68, c = 74.76 Å, β = 93.29°. Data-collection statistics are listed in Table 1. The Matthews coefficient (Matthews, 1968) was calculated to be 2.5 Å^3 Da^{-1} assuming the presence of four molecules per asymmetric unit, with a solvent content of 50.7%.

We used the structure of PdTIR (PDB entry 3h16; Chan *et al.*, 2009) as a template model for molecular replacement in *Phaser* (McCoy *et al.*, 2007). A promising solution was found with translation-function Z-scores above 20 and four molecules in the asymmetric unit. *Phaser* generated clean density for the majority of molecules in the asymmetric unit. However, parts of the density were missing from all four molecules. Model building and refinement are in progress. The structure of the TIR domain of TcpB should provide a sound foundation for a molecular understanding of how this protein affects the innate immune response of the host.

We are grateful to Daniel Ericsson for his help with data collection. We acknowledge the use of the Australian Synchrotron MX2 beamline and the UQ-ROCX Diffraction Facility. This work was supported by a grant from the National Health and Medical Research Council (NHMRC, Australia) to BK and AM. BK is an NHMRC Research Fellow. We thank the Majmaah University and the Ministry of Higher Education of Saudi Arabia for supporting the PhD scholarship for MA.

References

Bernoux, M., Ve, T., Williams, S., Warren, C., Hatters, D., Valkov, E., Zhang, X., Ellis, J. G., Kobe, B. & Dodds, P. N. (2011). *Cell Host Microbe*, **9**, 200–211.
Bowie, A. G. & Unterholzner, L. (2008). *Nature Rev. Immunol.* **8**, 911–922.
Chan, S. L., Low, L. Y., Hsu, S., Li, S., Liu, T., Santelli, E., Le Negrate, G., Reed, J. C., Woods, V. L. Jr & Pascual, J. (2009). *J. Biol. Chem.* **284**, 21386–21392.
Chan, S. L., Mukasa, T., Santelli, E., Low, L. Y. & Pascual, J. (2010). *Protein Sci.* **19**, 155–161.
Chaudhary, A., Ganguly, K., Cabantous, S., Waldo, G. S., Micheva-Viteva, S. N., Nag, K., Hlavacek, W. S. & Tung, C. S. (2012). *Biochem. Biophys. Res. Commun.* **417**, 299–304.
Cirl, C., Wieser, A., Yadav, M., Duerr, S., Schubert, S., Fischer, H., Stappert, D., Wantia, N., Rodriguez, N., Wagner, H., Svanborg, C. & Miethke, T. (2008). *Nature Med.* **14**, 399–406.
Eschenfeldt, W. H., Lucy, S., Millard, C. S., Joachimiak, A. & Mark, I. D. (2009). *Methods Mol. Biol.* **498**, 105–115.
Evans, P. (2006). *Acta Cryst.* D**62**, 72–82.
Gay, N. J. & Gangloff, M. (2007). *Annu. Rev. Biochem.* **76**, 141–165.
Kabsch, W. (2010). *Acta Cryst.* D**66**, 125–132.
Kawai, T. & Akira, S. (2007). *Semin. Immunol.* **19**, 24–32.
Kempkes, R., Stofko, E., Lam, K. & Snell, E. H. (2008). *Acta Cryst.* D**64**, 287–301.
Khan, J. A., Brint, E. K., O'Neill, L. A. & Tong, L. (2004). *J. Biol. Chem.* **279**, 31664–31670.
Lin, Z., Lu, J., Zhou, W. & Shen, Y. (2012). *PLoS One*, **7**, e34202.
Matthews, B. W. (1968). *J. Mol. Biol.* **33**, 491–497.
McCoy, A. J., Grosse-Kunstleve, R. W., Adams, P. D., Winn, M. D., Storoni, L. C. & Read, R. J. (2007). *J. Appl. Cryst.* **40**, 658–674.
McPhillips, T. M., McPhillips, S. E., Chiu, H.-J., Cohen, A. E., Deacon, A. M., Ellis, P. J., Garman, E., Gonzalez, A., Sauter, N. K., Phizackerley, R. P., Soltis, S. M. & Kuhn, P. (2002). *J. Synchrotron Rad.* **9**, 401–406.
Newman, R. M., Salunkhe, P., Godzik, A. & Reed, J. C. (2006). *Infect. Immun.* **74**, 594–601.
Nyman, T., Stenmark, P., Flodin, S., Johansson, I., Hammarström, M. & Nordlund, P. (2008). *J. Biol. Chem.* **283**, 11861–11865.
Ohnishi, H., Tochio, H., Kato, Z., Orii, K. E., Li, A., Kimura, T., Hiroaki, H., Kondo, N. & Shirakawa, M. (2009). *Proc. Natl Acad. Sci. USA*, **106**, 10260–10265.
Radhakrishnan, G. K. & Splitter, G. A. (2010). *Biochem. Biophys. Res. Commun.* **397**, 59–63.
Radhakrishnan, G. K., Yu, Q., Harms, J. S. & Splitter, G. A. (2009). *J. Biol. Chem.* **284**, 9892–9898.
Rana, R. R., Zhang, M., Spear, A. M., Atkins, H. S. & Byrne, B. (2012). *Med. Microbiol. Immunol.* **202**, 1–10.
Salcedo, S. P., Marchesini, M. I., Lelouard, H., Fugier, E., Jolly, G., Balor, S., Muller, A., Lapaque, N., Demaria, O., Alexopoulou, L., Comerci, D. J., Ugalde, R. A., Pierre, P. & Gorvel, J.-P. (2008). *PLoS Pathog.* **4**, e21.
Sengupta, D., Koblansky, A., Gaines, J., Brown, T., West, A. P., Zhang, D., Nishikawa, T., Park, S.-G., Roop, R. M. II & Ghosh, S. (2010). *J. Immunol.* **184**, 956–964.
Snyder, G. A., Cirl, C., Jiang, J., Chen, K., Waldhuber, A., Smith, P., Römmler, F., Snyder, N., Fresquez, T., Dürr, S., Tjandra, N., Miethke, T. & Xiao, T. S. (2013). *Proc. Natl Acad. Sci. USA*, **110**, 6985–6990.
Studier, F. W. (2005). *Protein Expr. Purif.* **41**, 207–234.
Valkov, E., Stamp, A., Dimaio, F., Baker, D., Verstak, B., Roversi, P., Kellie, S., Sweet, M. J., Mansell, A., Gay, N. J., Martin, J. L. & Kobe, B. (2011). *Proc. Natl Acad. Sci. USA*, **108**, 14879–14884.
Ve, T., Gay, N. J., Mansell, A., Kobe, B. & Kellie, S. (2012). *Curr. Drug Targets*, **13**, 1360–1374.
Winn, M. D. *et al.* (2011). *Acta Cryst.* D**67**, 235–242.
Xiao, T. S. (2010). *J. Clin. Immunol.* **30**, 638–642.
Xu, Y., Tao, X., Shen, B., Horng, T., Medzhitov, R., Manley, J. L. & Tong, L. (2000). *Nature (London)*, **408**, 111–115.
Yadav, M., Zhang, J., Fischer, H., Huang, W., Lutay, N., Cirl, C., Lum, J., Miethke, T. & Svanborg, C. (2010). *PLoS Pathog.* **6**, e1001120.